FABRICATION AND EVALUATION OF SHAPE MEMORY ALLOY PARTICLES DISPERSED TITANIUM COMPOSITES

Hiroyuki Toda, Takashi Hashizume and Toshiro Kobayashi
Department of Production Systems Engineering, Toyohashi University of Technology, Toyohashi, 441-8580, Japan

SUMMARY: TiNi particle dispersed Ti composite has been successfully produced by the spark plasma sintering method. The composite is initially subjected to a tensile prestrain below the reverse transformation temperature, and then, tensile loaded to failure above it after the unconstrained heating. The effects of the prestrain level, test and prestrain temperatures, and aspect ratio of the particle are evaluated by both the experiments and Eshelby equivalent inclusion method. Enhancement of the elevated temperature tensile properties due to the imposition of longitudinal compressive residual stress in the matrix is confirmed by the experiments and prediction. The predictions provide fairly good agreement with the experiments except that the strength and ductility are deteriorated in some conditions due to the damage evolution at brittle interfacial reaction layer. The most noticeable advantage of the shape memory alloy (SMA) dispersed composite is that even if the SMA phase is spherical, similar strengthening to the alighed fibrous composite can be achieved in contrast to the ceramic phase reinforced composites. The SMA particles exhibited spontaneous actuation during dynamic fracture of a notched specimen. This implies the feasibility of actuating such composites by local temperature elevation due to the plastic deformation of the matrix in the vicinity of a crack-tip, especially in the case of Titanium matrix composites which possesses low thermal conductivity.

KEYWORDS: Smart Composite, Shape Memory Alloy, Titanium, Particulate Composite, Strength, Spontaneous Actuation

INTRODUCTION

High strength composite materials are essential to the success of future transportation systems. In particular, titanium matrix composites offer significant opportunities for weight reduction in aircraft, aerospace and automotive applications. Recently, discontinuously-reinforced titanium[1] has emerged as an attractive and affordable alternative to conventional long fiber-reinforced composites due to its more isotropic and homogeneous properties, lower cost and applicability of conventional processes. However, improvement of strength by adding particles is relatively modest in titanium alloys. It is partly attributed to originally high strength of the unreinforced titanium alloys and limited kinds of available reinforcing particles due to interfacial chemical reaction. On the other hand, several attempts have recently been reported that SMA fibers were dispersed into an epoxy or an aluminum matrix

in order to enhance strength and toughness by shrinkage of the SMA above a transformation temperature[2]. A study was undertaken to examine whether such procedure is applicable to achieve substantial property improvements in titanium matrix DRMs. The present study also focuses on spontaneous actuation of the SMA phase without using any external sensors, processors, heating source and so forth. Plastic deformation of the matrix accompanying considerable local temperature rise in the vicinity of a crack-tip during dynamic fracture is utilized to actuate the SMA particles.

PROCEDURE

2.1 Experimental

Gas-atomized Ti-49.8at%Ni particles were supplied by Daido Steel Co., Ltd., in Nagoya, Japan. The particles were almost spherical and less than 100μm in diameter. –325 mesh 99.9at% Ti powder was blended with the SMA powder, and composites were made up using the techniques of spark plasma sintering at 923K for 100s at a pressure of 49MPa to contain 20vol% TiNi. The samples were annealed at 773K for 3.6ks and then cooled to 243K to transform the whole TiNi particles to martensite phase. SEM microscopy has been carried out on polished samples, using energy dispersive X-ray analyzer. Microindentations have also been made using a Vickers indenter with a 0.49N load to investigate its temperature dependency. Transformation temperatures after and before the consolidation were measured by DSC. Tensile specimens were machined from consolidated compacts of 30 mm in diameter using electro-discharge machining, followed where appropriate by mechanical polishing. The specimens were subjected to a tensile prestrain at low temperature (i.e. $T<A_s$), then, heated to high temperature (i.e. $T>>A_f$) after unconstraining by unfastening grips, and finally tensile loaded to failure at the temperature. The low and high temperatures here are 325 and 473K, respectively, unless otherwise specified. The tensile tests were performed on specimens of cross section 4 x 1 mm using an universal testing machine (Instron model 5583) at a loading rate of 8.33 x 10^{-6} m/s. The in-situ studies were also undertaken in a SEM, which has a straining stage of 2kN in the maximum capacity. In addition, notched specimens of three point bending bar were also machined to investigate feasibility of actuating the SMA particles by temperature rise at a crack-tip. The tests were performed using a servo-hydraulic impact testing machine (Shimazu model EHF-U5H-20L) at a loading rate of 12 m/s. The phase compositions of fracture surfaces are studied using X-ray diffraction immediately after the fracture. The temperature of the specimens was controlled to be kept between 327 and 331K from the impact test through the X-ray diffraction measurement.

2.1 Analytical Procedure

Residual stresses and composite yield strength were analyzed on basis of the Eshelby equivalent inclusion method which were proposed by Taya et al. for SMA fiber MMCs[2]. After solving eq.(1) at 325K to calculate uniform plastic strain of the particle, $\tilde{e}_{pl}$, eq.(2) was solved to predict the composite yield strength.

$$\tilde{\sigma}_0+\tilde{\sigma}=\tilde{C}_p\cdot\left(\tilde{e}_0+\bar{\tilde{e}}+\tilde{e}+\tilde{e}_{pl}\right)=\tilde{C}_m\cdot\left(\tilde{e}_0+\bar{\tilde{e}}+\tilde{e}-\tilde{e}^*\right) \quad (1)$$

$$\tilde{\sigma}_0+\tilde{\sigma}=\tilde{C}_p\cdot\left(\tilde{e}_0+\bar{\tilde{e}}+\tilde{e}+\tilde{\varepsilon}_T-\tilde{\varepsilon}_{pl}+\tilde{e}_{pl}\right)=\tilde{C}_m\cdot\left(\tilde{e}_0+\bar{\tilde{e}}+\tilde{e}-\tilde{e}^*\right) \quad (2)$$

where tilda denotes tensor, $\tilde{\sigma}_0$ and $\tilde{\sigma}$ are far field loading and internal stress field occurred by the transformation of the SMA, respectively. $\tilde{C}_p$ and $\tilde{C}_m$ are stiffness tensors of the SMA particle and matrix, respectively. $\tilde{e}_0$ corresponds to $\tilde{\sigma}_0$ through $\tilde{C}_m$, and $\tilde{\tilde{e}} + \tilde{e}$ is internal strain. The SMA particles were assumed to shirink by $\tilde{\varepsilon}_T$, by which the matrix or particles deforms plastically by $\tilde{\varepsilon}_{pl}$ without any applied loading. $\tilde{e}_{pl}$ is plastic strain of the Ti matrix by far-field-loading $\tilde{e}^*$ is an unknown eigenstrain which is usually used in the equivalent inclusion method. In the present study, the von Mises yield criterion and the concept of energy balance proposed by Taya et al. were used to solve the eq. (2). Details of the procedure is available elsewhere[2]. The TiNi physical properties were obtained from ref.[2].

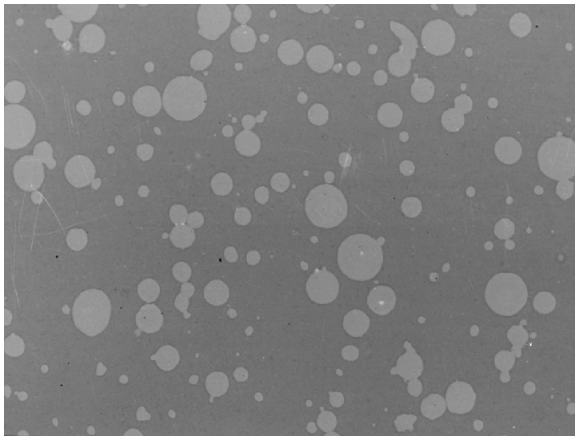

Fig.1 SEM micrograph of the Ti-20vol%TiNip composite.

RESULTS AND DISCUSSION

3.1 Microstructure and basic characteristics of the composite

Figure 1 shows typical morphology and spatial distribution of the TiNi particles. It has been demonstrated that the TiNi morphology remains completely spherical even after the consolidation. It has to be assumed that the consolidation was presumably achieved by deformation and/or local melting of the Ti powder. There was no evidence of considerable agglomeration and any other fabrication defects except that there was some residual porosity visible adjacent to a fusion line between connected TiNi particles. Measured relative density was 98.2%, which seems to be worth evaluating its mechanical properties experimentally. Fig.2 shows results of the SEM-EDX line analysis. It is evident that the SPS process has led

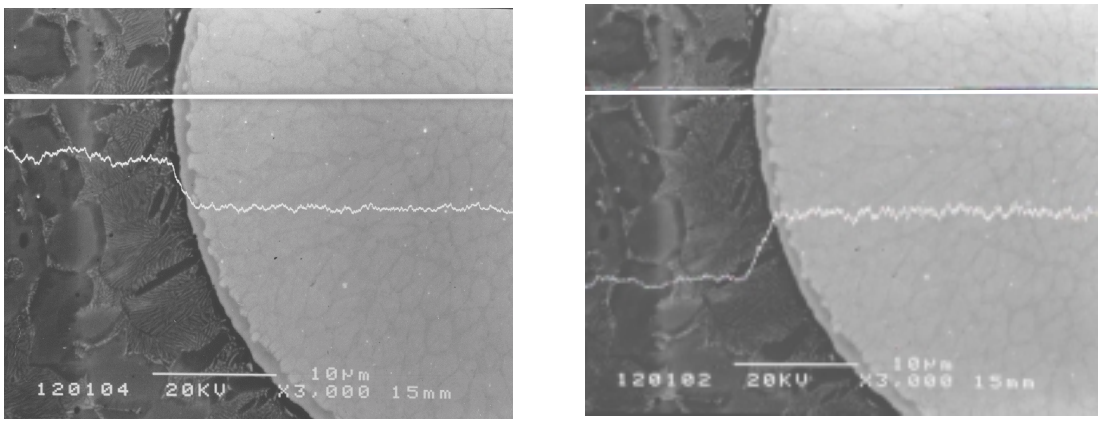

(a) Ti (b) Ni

Fig.2 Results of the SEM-EDX line analyses.

to an interfacial reaction layer of about 1μm in thickness at each particle. Scanning electron microscopy of the layer by EDX spectroscopy has confirmed that it is Ti_2Ni. Enrichment of Ti in the vicinity of the TiNi particle and that of Ni in the matrix adjacent to the interface can be also seen in Fig.2.

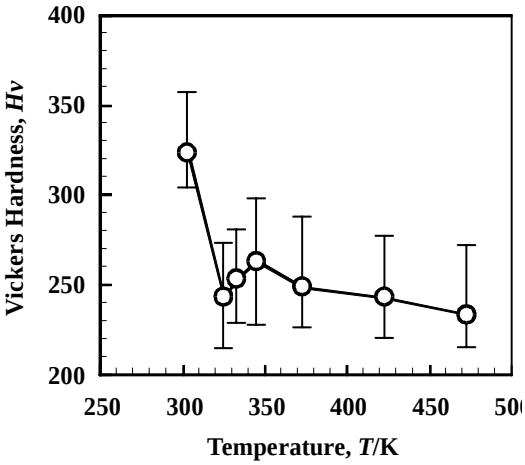

Fig.3 Variations of Vickers hardness of the particles in the Ti-20vol%TiNip composite as a function of temperature.

Start and finish temperatures of martensite transformation, M_s and M_f, and those of reverse transformation of the martensite, A_s and A_f, were 325, 303, 333 and 345K, respectively, in the composites. These temperatures were 20~32K higher than those before the consolidation. This may be attributed to the increase in average Ti concentration within the TiNi phase. Fig.3 shows variations of Vickers hardness at TiNi particles as a function of temperature. The hardness decreases rapidly until 325K with the increase of temperature and then gradually decreases from 345K. Existence of the minimal value at Ms (i.e. 325K) agrees well with the reported tendency of yield stress variation in the literature[3].

3.2 Strengthening of the composites by shrinkage of the SMA particles

After subjecting specimens to tension to 413 - 671 MPa at 325K, macroscopic residual strains of 0.03 - 0.28% were generated. Note that the macroscopic residual strains are different from inelastic strain within the particle, $\tilde{\bar{e}}_{pl}$. For example, $\tilde{\bar{e}}_{pl}$ is 0.0086 for the macroscopic prestrain of 0.20% and it is already 0.0043 for 0.28%. Then the specimens were tested in tension at 473K and variation of the 0.1% proof stress as a function of prestrain is plotted in Fig.4. Included are the predictions by the micromechanics. It should be noted here that the apparent plastic strain of the SMA particles predicted by eq. (1) is so small that neither the matrix nor particles can yield at 473K before application of far-field loading. Increment of 0.1% proof stress due to the shrinkage of the SMA particles reaches about 71MPa at the macroscopic prestrain of 0.20%, while further prestraining up to 0.28% gives rise to any increase in the strength and ductility. The predicted maximum increment in the 0.1% proof stress is about 91MPa, which is comparable to the experimentally obtained value. However, the prediction underestimates the yield strength

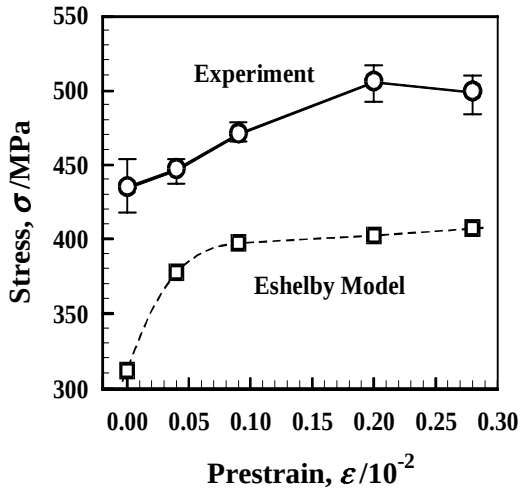

Fig.4 0.1% proof stress of the Ti-20vol%TiNip composites at 473K as a function of prestrain applied at 325K.

over all of the experimental conditions performed in this study. One possible explanation for the discrepancy may be the definitions of the yield stress. The Eshelby model predicts the onset of yielding on basis of the von Mises yield criterion, while the measured offset proof stress corresponds to rather later stage where the effects of the work hardening are involved

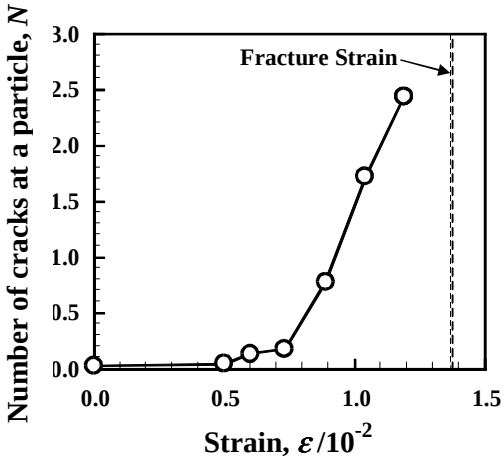

Fig.5 Accumulation of damage at each particle with the increase in strain.

The decrease in the proof stress after straining up to 0.28% is attributed to multiple cracking of the interfacial reaction layer as shown in Fig.5. Clearly the result shows that the damage accumulation rate is considerably high at applied strains above 0.7, which still corresponds to the early stage of plastic deformation at 325K. According to a SEM micrograph taken from polished specimen surface during loading, multiple cracking in the interfacial reaction layer can be seen. TiNi appears to be the most ductile phase, being never cracked throughout the tests. Actually, the ductile TiNi particles plays a role as a crack arrester, thereby the microcracks initiated at the interfacial reaction zones propagates only into the Titanium matrix, being perpendicular to the loading axis. In addition, since the microcracks are formed predominantly near an equator of each particle, the existence of a limited number of the microcracks seems to have almost a negligible effect on composite flow curve at 473K. Of course, the prestrain level of 0.28% exceeds such limits.

Figure 6 (a) represents the effects of the test temperature above A_f, which mainly reflects variations of the yield stress of both the matrix and SMA particle. The 0.1% proof stress

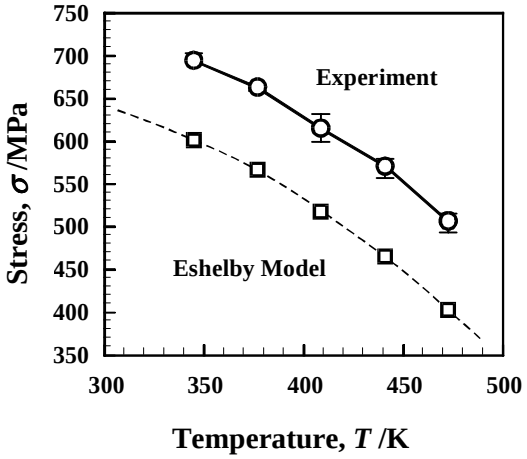

(a) 0.1% proof stress

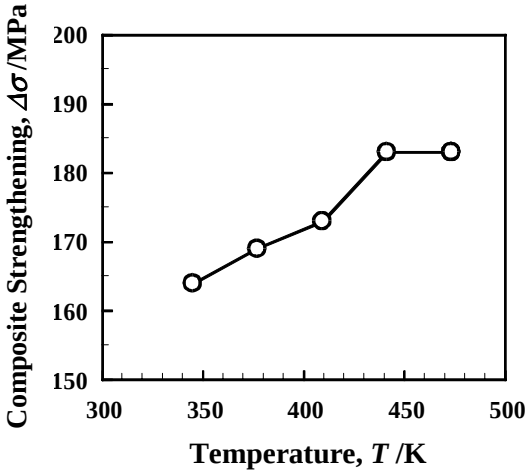

(b) Composite strengthening

Fig. 6 (a) Composite yield strength as a function of temperature, together with the prediction by the Eshelby model. Strengthening by the addition of the TiNi is also shown in (b)

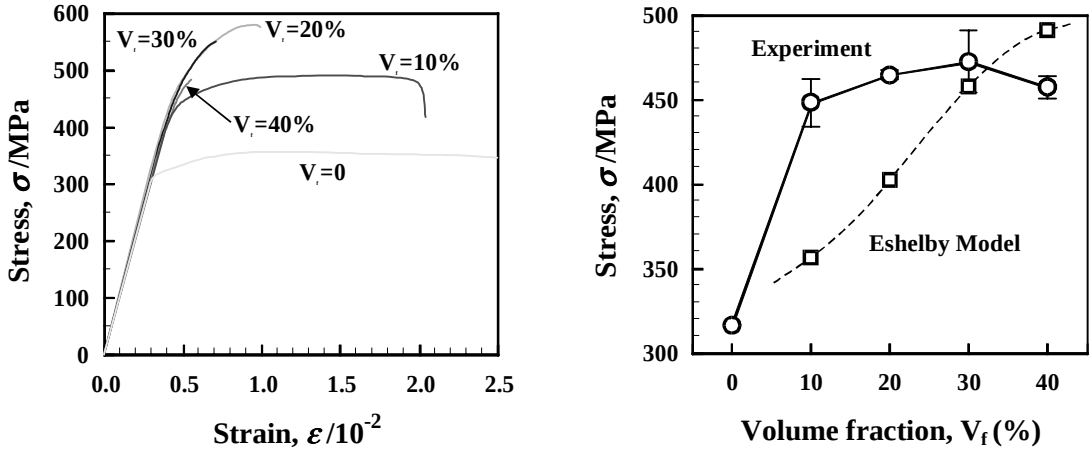

(a) Stress-Strain Curves **(b) 0.1% Proof Stress**

Fig.7 Effects of particle volume fraction on stress-strain relationship.

decreases monotonously with the increase of temperature. Both the experiment and prediction indicate comparable trends despite the fact that there also exists the underestimation. Since the 0.1% proof stress of the unreinforced Titanium decreases rapidly from 597 to 323MPa between 325 and 473K, compensating for the reduction in the matrix proof stress is necessary to evaluate effects of the SMA particle. Fig.6 (b) represents data corrected for such weakening of the matrix, which clearly shows increasing efficiency with the temperature rise.

Figure 7 shows the effects of the particle volume fraction. There are two features to note on the effects of the particle volume fraction. When the particle volume fraction is less than 20%, the stress-strain curve is displaced to the upper direction with the increase in volume fraction. The second feature to note is no discernible elevation in the flow stress level above 20vol%. On the contrary, fracture occurred at early stages by that the stress strain curves were broke off immediately after the elastic limit. Indeed, since the 0.1% proof stress could not be measured in the case of 40vol%, the comparison between the prediction and measurement is shown by 0.05% proof stress in Fig.7(b). As the volume fraction increases, the difference between them reduced gradually and the values reversed at 40vol%. The latter tendency may be due to the damage evolution at the interface. There is clearly need for further work in order to suppress the formation of the brittle layer. This may be possibly achieved by protecting the TiNi particles by a suitable coating of much slower

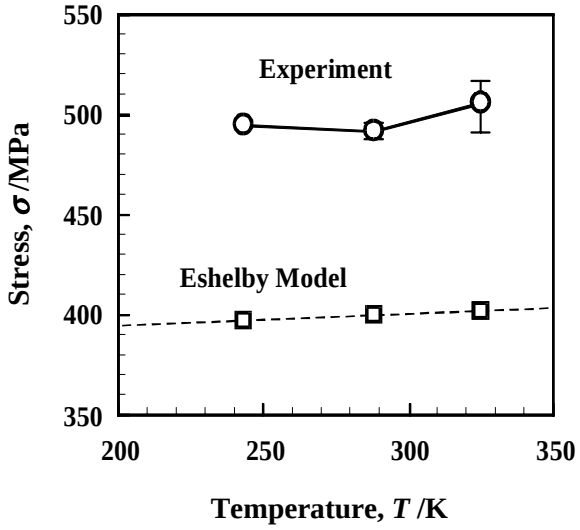

Fig.8 0.1% proof stress of the Ti-20vol%TiNip composites at 473K as a function of temperature at which the prestrain is applied.

diffuser or oxidization of the particle surface.

Figure 8 shows the effects of prestraining temperature on the composite strength. Lowering the temperature may bring two significant affects; decreases in both the matrix and TiNi strengths. The reduction in the matrix strength lowers the composite strength, while that of the apparent yield strength of the SMA phase enhances the composite strengthening as shown in Fig.9 by increasing the inelastic strain at the particles for the same macroscopic applied strain. The latter is simply because the recovery strain of the SMA particles is proportional to the apparent plastic strain at 325K. Generally, the yield stress of the SMA has a minimum in the vicinity of M_s temperature[3]. Above the M_s temperature, the yield stress rapidly increases with increasing temperature, while it increases gradually with decreasing temperature below the M_s temperature[3]. In this study, only the effects of the matrix strength was accounted for in the prediction of Fig.8, because the mechanical properties of the bulk TiNi could not be measured. Nevertheless, agreement between the measured and predicted tendencies is excellent, suggesting that the variation of the yield strength of SMA is almost negligible within the temperature range tested. This may be attributed to the in-situ increase of the Ms temperature in the composite.

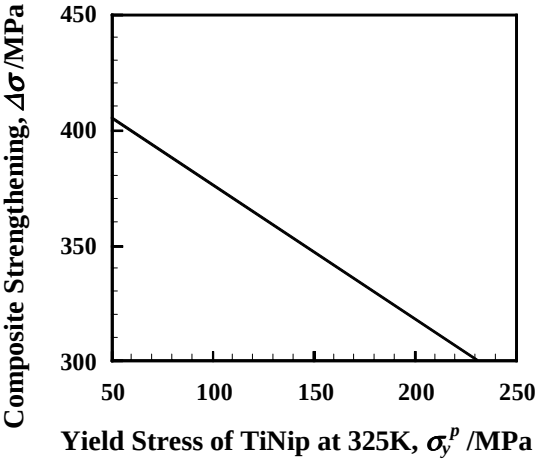

Fig.9 Prediction of the composite yield strength as a function of yield strength of the TiNi particle at 325K.

Figure 10 shows the effects of aspect ratio of the SMA particles on the composite yield stress. The critical prestrain does not change noticeably above the aspect ration of 5, approaching a limiting value for an infinite long fiber. In addition, it should be noted here that the composite yield stress does not change to discernible extent by the aspect ratio after the prestain reaches the critical values. This implies that elongation of the particles is effective only for the reduction of the critical prestrain, thereby substantial amount of the recovery stress can be obtained even if the interfacial reaction produces the brittle interphase to some extent. The feature represented here clarifies an advantage of the SMA dispersed composite well. Generally, in the case of ceramic particles dispersed composites, strength of long fiber reinforced composites is much higher

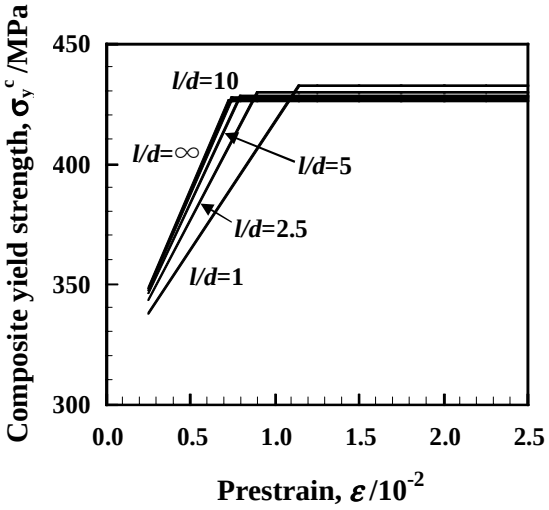

Fig.10 Prediction of composite yield stress at 473K as a function of prestrain at 325K.

than that of the particle dispersed composites. This is attributed to that the particle stress is remarkably suppressed in comparison to the long fiber because of the insufficient load transfer from a matrix. In contrast, it should be emphasized that the particulate SMA can generate the similar recovery stress with the fibrous SMA if sufficient prestrain is applied to the particle, thereby realizing superior mechanical properties.

3.3 Feasibility of actuating the SMA particles by heat generation in the vicinity of a crack-tip

The XRD spectra of the fracture surfaces after testing at static and dynamic loading rates are presented in Fig.11. It could be seen that the phase compositions after the static fracture closely fit the data before the test, while reverse transformation to Austenite can be detected after the fracture at the loading rate of 12m/s. It suggests that there occurred sufficient amount of heat generation during the test. Generally, plastic deformation near the tips of stationary and running cracks accompanies local temperature elevations[4]. Especially, in the case of Titanium, the temperature rise is higher than that for steel by a factor of six for the same stress intensity factor[4]. According to the solution proposed by Rice et al.[4], the temperature rise, ΔT, within a plastic zone ahead of a stationary crack after loading from 0 to t_{Pmax} (Time to the maximum load) for a non-hardening material is given as follows;

$$\Delta T \propto K^2 \Big/ E\sqrt{\rho c \kappa t_{P_{\max}}} \tag{3}$$

where K is stress intensity factor, E is Young's modulus, ρ is density, κ is thermal conductivity, and c is heat capacity. The temperature rise for 12m/s is calculated to be about 475K. The calculation may support the reverse transformation observed in Fig.11. However, heat transfer should be taken into consideration as rate controlling step of the reverse

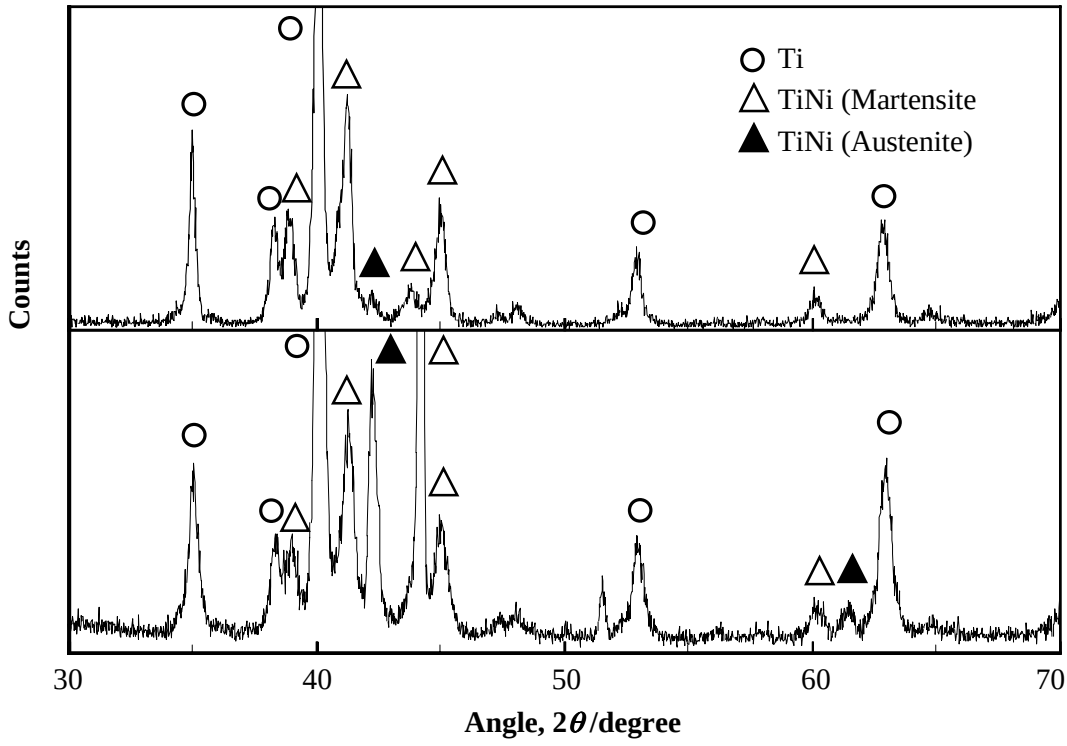

Fig.11 X-ray diffraction patterns of fracture surfaces after the tensile tests at static and dynamic loading rates.

transformation during the high speed loading. In this study, t_{Pmax} for the loading rate of 12m/s was 664μs. On the other hand, according to the Gurney diagram which gives temperature rise due to heat transfer from surface of a sphere[5], it takes about 83μs for temperature rise from 330 to 350K at a TiNi sphere of 100 μm in diameter from the moment that the sphere is immersed into the substance of 400K. Since this is enough short in comparison to the time necessary for the fracture, the above-mentioned interpretation of the reverse transformation can be validated. Such instantaneous shrinkage of the SMA phase leads to offset of crack-tip stresses by the shrinkage of each particle in the exactly opposite direction of the stress field which significantly reduces the crack-tip stress intensity, thereby enhancing fracture toughness of the cracked-body effectively. Future efforts may well see experimental verification of such mechanism utilizing accurate fracture toughness testing.

CONCLUSION

1) TiNi particle dispersed Ti composite has been successfully produced by the spark plasma sintering method. The TiNi particle remained to be spherical. Relative density reached about 98.2%. The Ti_2Ni layer of about 1μm in thickness was formed at the TiNi/Ti interface as a result of the chemical reaction during the fabrication process.
2) Firstly the composite was prestrained below the reverse transformation temperatures, and then, its tensile properties were measured above it. The effects of the prestrain level, testing and prestraining temperatures, and aspect ratio of the particle were evaluated by both the experiment and Eshelby equivalent inclusion method. Enhancement of tensile properties due to the generation of compressive residual stress in the matrix was confirmed both by the experiments and prediction. The predictions agree well with the experiments except that the strength and ductility were deteriorated when large prestrain was applied or the particle volume fraction was high. This was attributed to the interfacial damage evolution at the brittle Ti_2Ni layer.
3) Even if TiNi is spherical, similar strengthening to the alighed fibrous composite can be achieved in the shape memory alloy dispersed composite. It presents a contrast with the ceramic phase reinforced composites in which long fiber reinforced composites are far stronger than particulate composites. This implies that elongation of the particles is effective only for the reduction of the critical prestrain.
4) Spontaneous actuation of the shape memory alloy phase was observed during dynamic fracture. Heat source for the actuation is considered to be plastic deformation of the matrix in the vicinity of a crack-tip which accompanies considerable local temperature elevation in the case of Titanium matrix.

ACKNOWLEDGEMENTS

The authors would like to thank Dr. T.Shimizu at Daido Steel Co., Ltd. for providing the TiNi powder, and Dr. M.Otake at Shizuoka Industrial Research Institute for the use of apparatuses for the sample preparation.

REFERENCES

1. Saito T., Furuta T. and Yamaguchi T., *Recent Advances in Titanium Metal Matrix Composites*, Ed. By Froes F.H. and Storer J., TMS, Pittsburg, USA, 1995, 33-44.
2. Taya M., Shimamoto A. and Furuya Y., *Proc. of ICCM-10*, Whistler, B.C., Canada, 1995, V-275-282.
3. Honma T., *Shape Memory Alloys*, Ed. by Funakubo H., Gordon and Breach Service Publishers, New York, USA, 1987, 77.
4. Rice J.R. and Levy N., *Physics of Strength nd Plasticity*, Eds. by A.S.Argon, MIT Press, 1969, 277-293.
5. Gurney H.P. and Lulie J.: *Ind. Eng. Chem*., Vol.15, 1923, 1170-1172.